[*Electronic Supporting Information*]

Construction of cationic organic network for highly efficient removal of anionic contaminants from water

Zhi-Jun Li,*[, a] Hua-Dong Xue,[b] Yu-Quan Zhang,[a] Huai-Sheng Hu,[a] and Xu-Dong Zheng*[, a]

[a] *College of Chemistry and Chemical Engineering, Longdong University & FLUOBON Collaborative Innovation Center, Longdong University, Qingyang, Gansu, 745000, P. R. China.*

[b] *State Key Laboratory of Applied Organic Chemistry, College of Chemistry and Chemical Engineering, Lanzhou University, Lanzhou, Gansu 730000, P. R. China.*

*E-mail: lizhj_chem@163.com; zhengxd1961@126.com

A. Summary of Figures and Tables

B. Materials and Instrumentation

Materials

All reagents, unless otherwise stated, were purchased from commercial sources and used without further purification.

Instrumentation

Elemental analysis was carried out on a VarioEL V3.00 elemental analyzer (Elementar Analysensysteme GmbH). Powder X-ray diffraction (PXRD) data were collected with a PANalytical X'Pert Pro Diffractometer operated at 40 kV and 40 mA with Cu Kα radiation (step size of 0.017°, step time of 8.40 s). Fourier transform Infrared (FT-IR) spectra were recorded on a Shimadzu 8400S instrument. Solid-state NMR measurements were performed on a Bruker WB Avance II 400 MHz spectrometer. The ^{13}C CP-MAS NMR spectra were recorded with a 4-mm double-resonance MAS probe and with a sample spinning rate of 10.0 kHz; a contact time of 2 ms (ramp 100) and a pulse delay of 3 s were applied. Scanning Electron Micrograph (SEM) images were obtained with a Hitachi S-4800 microscope operated at an accelerating voltage of 5.0 kV. The samples were prepared by dropping the suspension of material in ethanol on a silicon pellet, then dried and coated with gold. The thermogravimetric analysis (TGA) was performed on a Perkin Elmer instrument over the temperature range of 50 to 600 °C with a heating rate of 10 °C/min under nitrogen atmosphere. The nitrogen adsorption and desorption isotherms were measured at 77 K using a Micromeritics ASAP 2020M system. Surface areas were calculated from the adsorption data using Brunauer-Emmett-Teller (BET) method. The pore-size-distribution were calculated from the adsorption branches using non-local density functional theory (NLDFT) method. UV-Vis spectra were recorded on an Agilent Cary 60 Spectrophotometer.

C. Synthetic Procedure

Synthesis of CON-1

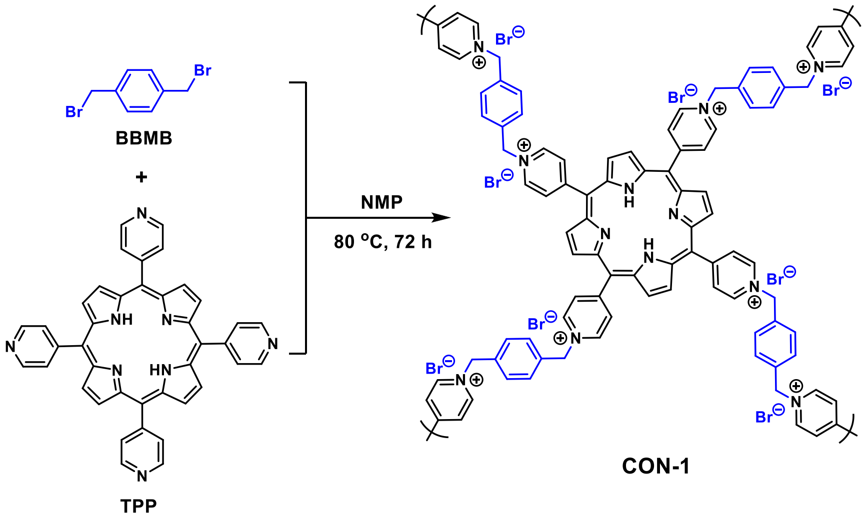

To a single-necked flask were added 1,4-bis(bromomethyl)benzene (BBMB, 0.2 mmol, 52.8 mg) and 5,10,15,20-tetra(4-pyridyl)porphyrin (TPP, 0.1 mmol, 61.9 mg). The solvent N-methyl pyrrolidone (5 mL) was added *via* injection under N_2 atmosphere. The reaction mixture was stirred and heated at 80 °C for 72 hours. After cooling to the room temperature, the obtained solid was transferred into a vial and washed with methanol, water, acetone, DMF, and THF. The solid was further purification by Soxhlet extraction in methanol for 48 hours, then dried at 90 °C for 8 hours to yield **CON-1** as dark purple powder, 91.0 mg, yield: 79 %. Elemental analysis (%): Calcd. for $[C_{56}H_{42}Br_4N_8]_n$: C 58.66; H 3.69; N 9.77. Found: C 57.76; H 4.28; N 8.88.

D. FT-IR Spectra

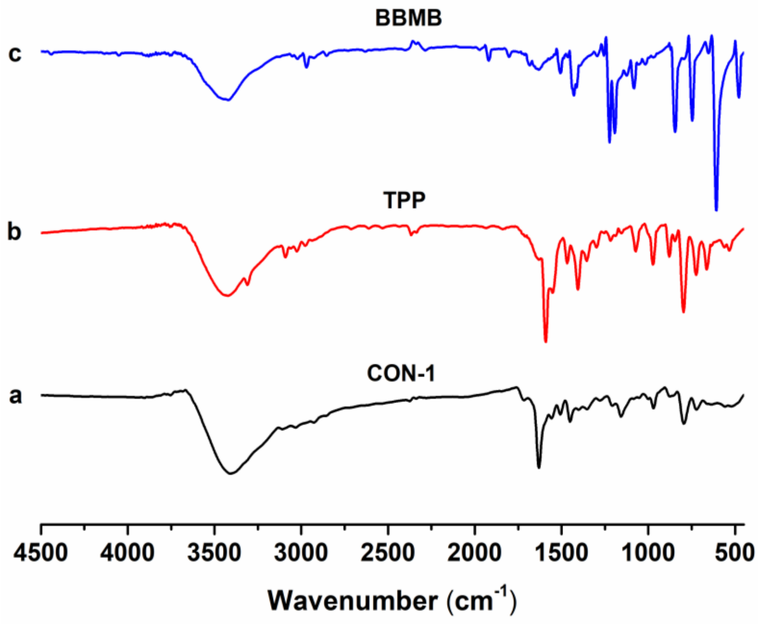

Figure S1. FT-IR spectra of **CON-1** (a), 5,10,15,20-tetra(4-pyridyl)-porphyrin (b, TPP), and 1,4-bis(bromomethyl)benzene (c, BBMB).

E. ^{13}C CP-MAS NMR Spectra

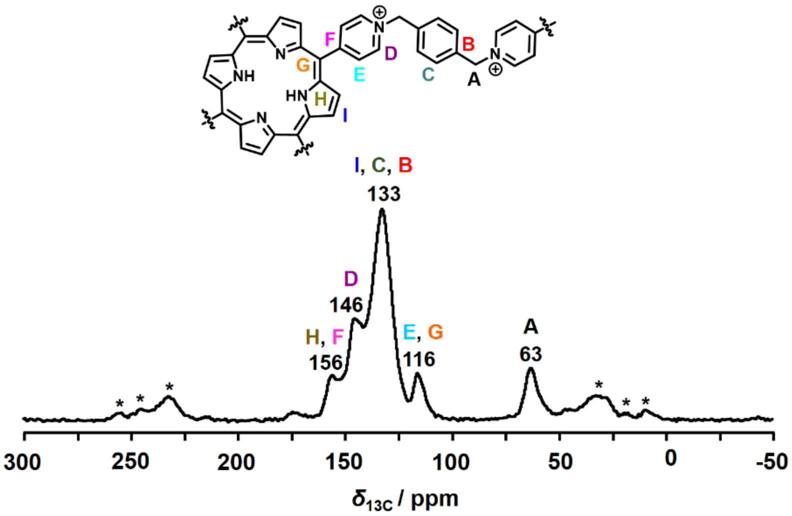

Figure S2. Solid state ^{13}C CP-MAS NMR spectrum of **CON-1**. The asterisks denote the spinning sidebands. The assignments of chemical shifts in **CON-1** were indicated in the chemical structure.

F. Powder X-ray Diffraction Analysis

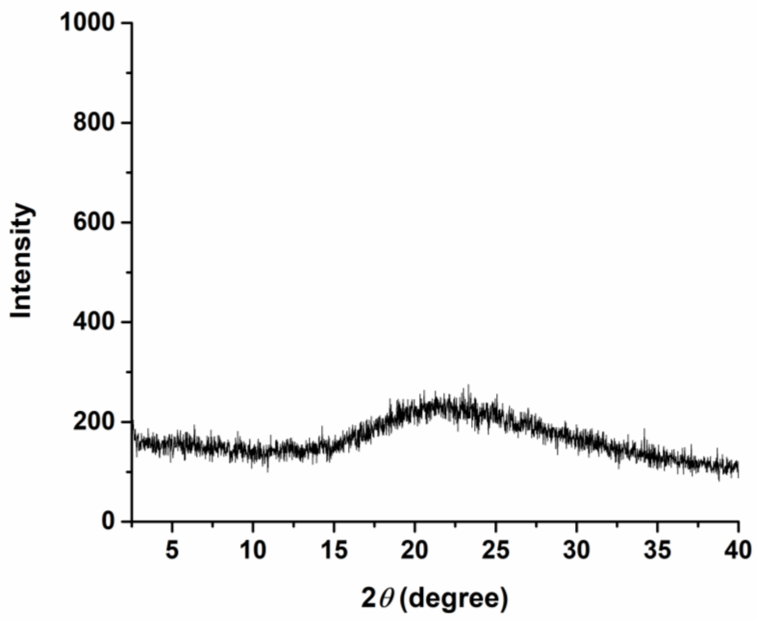

Figure S3. Powder X-ray diffraction (PXRD) pattern of **CON-1**. The broad peak around 23° in the PXRD pattern indicated the amorphous structure of **CON-1**.

G. N_2 Adsorption-Desorption Analysis

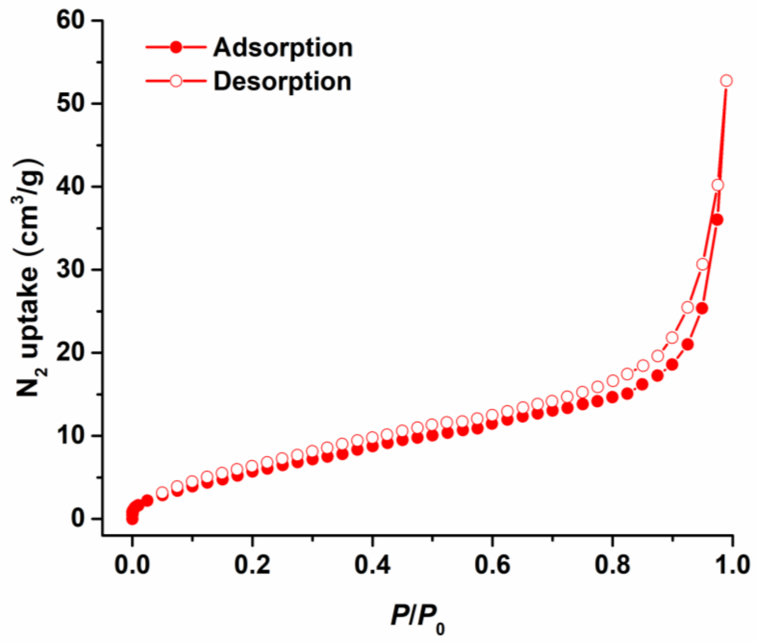

Figure S4. N_2 adsorption and desorption isotherms of **CON-1**.

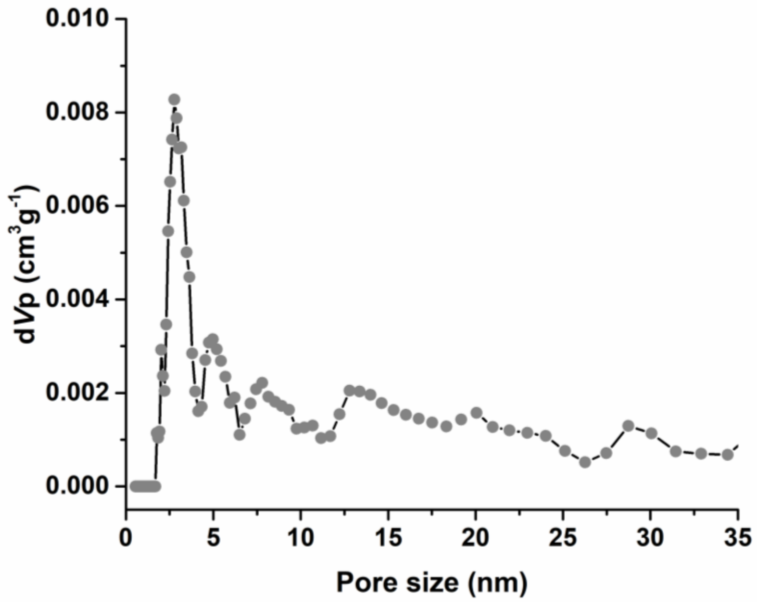

Figure S5. Pore-size-distribution of **CON-1** calculated from the adsorption isotherm with NLDFT method.

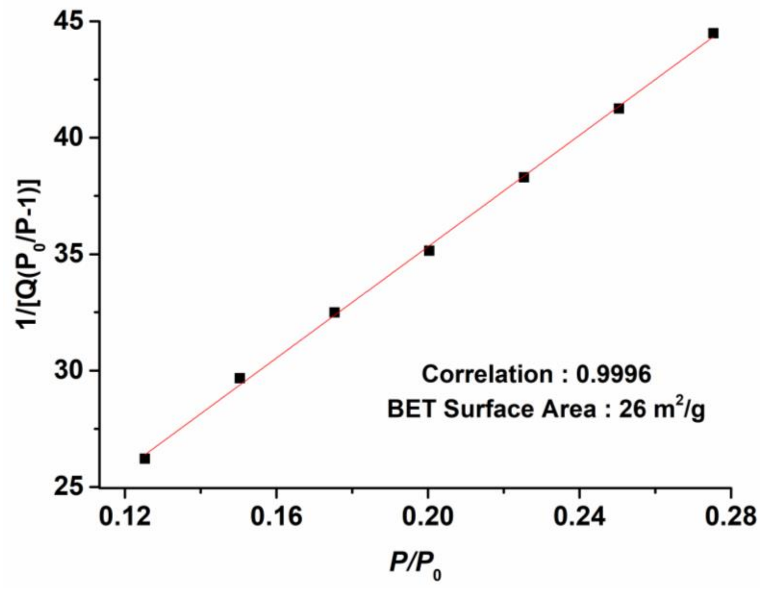

Figure S6. BET surface area plot for **CON-1** calculated from the adsorption isotherm.

H. Thermogravimetric Analysis

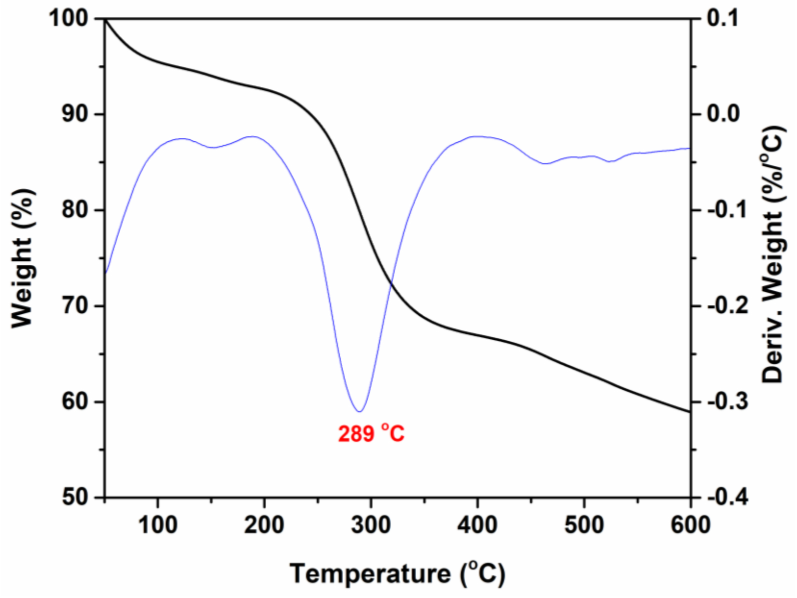

Figure S7. The TGA curve of **CON-1**. The TGA suggested that **CON-1** is thermostable to 289 °C under N_2 atmosphere.

I. Scanning Electron Micrographs

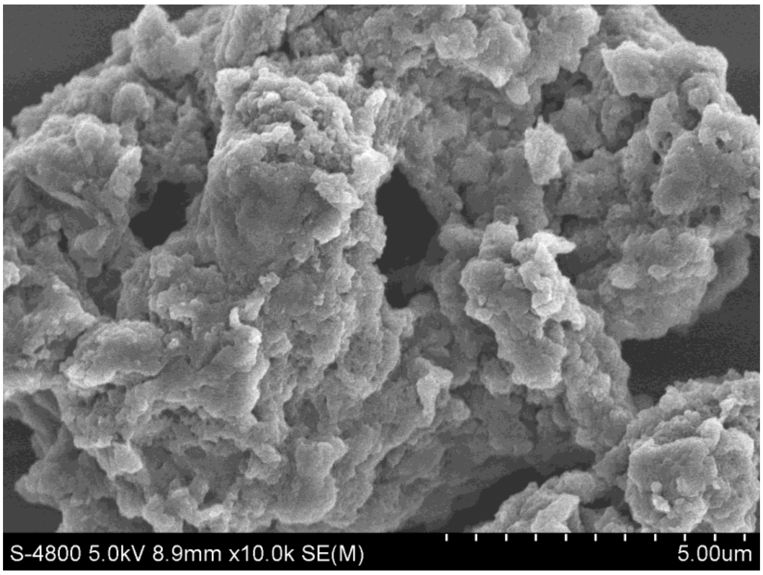

Figure S8. The SEM image of **CON-1**.

J. Organic Dyes Adsorption Experiments

General procedure for the organic dyes adsorption experiments

In adsorption experiments, four organic dyes were employed, including orange G (OG), methylene blue (MLB), rhodamine B (RHB), and new coccine (NC). These organic dyes can be classified into two groups: anionic dyes (OG and NC) and cationic dyes (MLB and RHB). Generally, **CON-1** (2 mg) was immersed into 9 mL of dye aqueous solution (66 μM), and the suspension was separated by centrifugation at different time points, then the upper clear solution was pipetted and measured by UV-Vis spectrophotometer. After each measurement, the solution was poured back to the initial vial to keep the total amount of dye constant. The dye contents in the solution were calculated by comparing the maximum absorbance before and after adsorption. The kinetics data for adsorption of OG was fitted with pseudo-first order and pseudo-second order models respectively.

Pseudo-first order equation:

$$Q_t = Q_e - Q_e e^{-k_1 t}$$

Pseudo-second order equation:

$$Q_t = \frac{k_2 Q_e^2 t}{1 + k_2 Q_e t}$$

The release experiment was carried out after the adsorption of OG dye is completed. The suspension was separated by centrifugation and the upper clear solution was replaced with the same volume of DMF solution containing $NaNO_3$ (128 mg), and monitored by UV-Vis measurements.

The adsorption capacity was evaluated by immersing **CON-1** (5 mg) in 6 mL OG aqueous solution with different concentrations (15 mg L^{-1}, 100 mg L^{-1}, 200 mg L^{-1}, 400 mg L^{-1}, 600 mg L^{-1}, 800 mg L^{-1}, and 1000 mg L^{-1}). After 12 hours, the adsorption reached equilibrium. By comparing the maximum absorbance of OG solution before and after adsorption, the equilibrium adsorption capacity can be calculated. The adsorption isotherm of OG was fitted with LangmuirEXT, Langmuir, and Freundlich models respectively.

LangmuirEXT equation:

$$Q_e = \frac{Q_m K_S C_e^{\gamma}}{1 + K_S C_e^{\gamma}}$$

Langmuir equation:

$$Q_e = \frac{Q_m K_L C_e}{1 + K_L C_e}$$

Freundlich equation:

$$Q_e = K_F C_e^{1/n}$$

Table S1. The structure information of organic dyes used in this contribution.

Structure	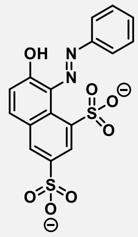	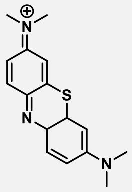	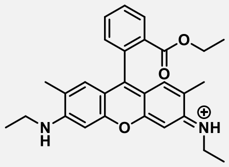	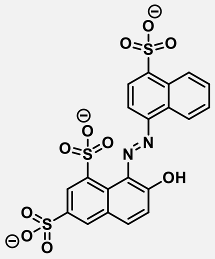
Name	Orange G	Methylene Blue	Rhodamine B	New Coccine
Abbr.	OG	MLB	RHB	NC
Charge	-2	+1	+1	-3
Mw.	452.37	373.90	479.01	604.47
Dimension (Å)	x = 5.44 y = 10.14 z = 15.64	x = 4.00 y = 7.93 z = 16.34	x = 6.53 y = 11.89 z = 15.55	x = 5.44 y = 10.48 z = 17.38

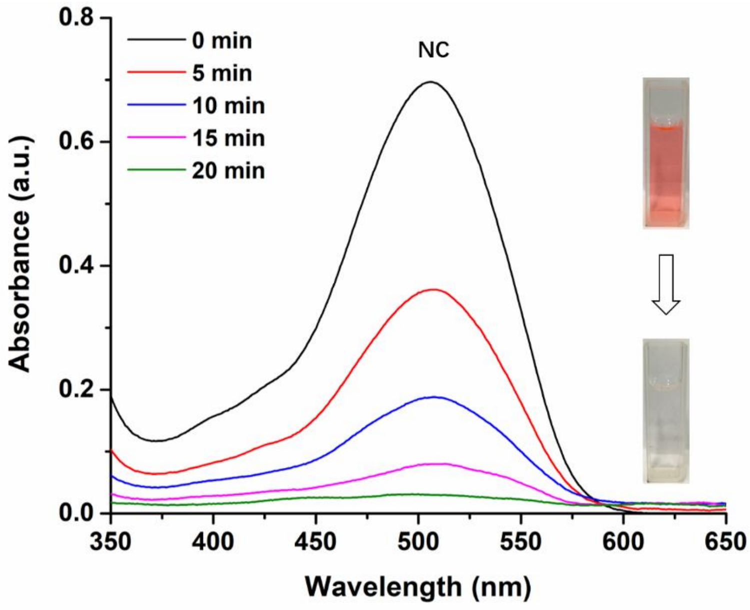

Figure S9. UV-Vis absorbance of NC aqueous solution in the presence of **CON-1** in different intervals.

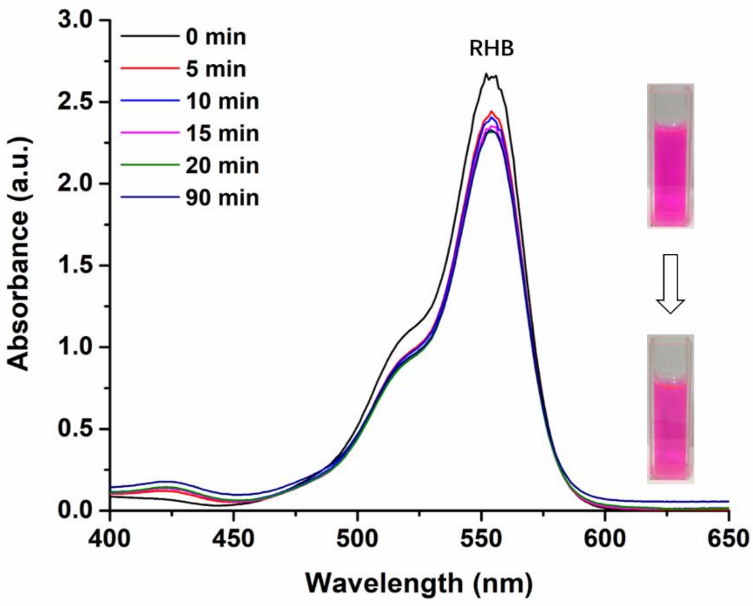

Figure S10. UV-Vis absorbance of RHB aqueous solution in the presence of **CON-1** in different intervals.

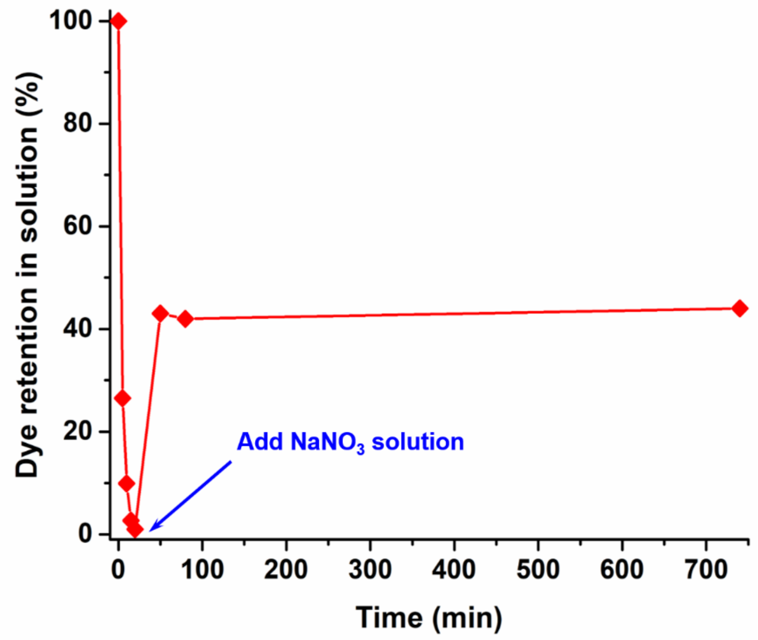

Figure S11. The content of OG in the release experiment. As shown in Figure S11, the adsorbed OG could not be fully released, which may because of the strong interaction between OG and the cationic framework of **CON-1**.

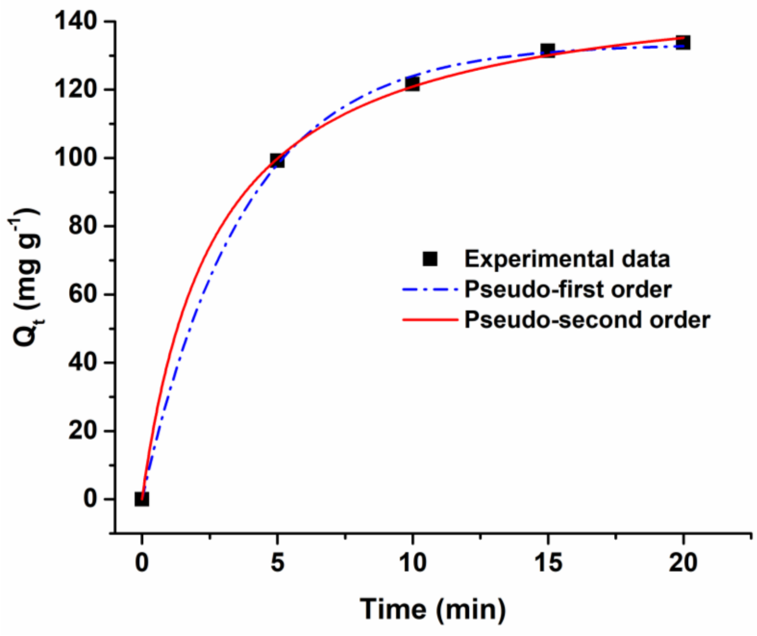

Fitting model	Parameter	correlation coefficient
Pseudo-first order	$Q_e = 133.4$ mg g^{-1} $k_1 = 0.266$ min^{-1}	$R^2 = 0.9993$
Pseudo-second order	$Q_e = 153.3$ mg g^{-1} $k_2 = 2.43 \times 10^{-3}$ g mg^{-1} min^{-1}	$R^2 = 0.9996$

Figure S12. The kinetics for adsorption of OG. The data was fitted with pseudo-first order equation and pseudo-second order models respectively. As listed in table above, pseudo-second order fitting gave a higher correlation coefficient, indicating the adsorption of OG followed the pseudo-second order model.

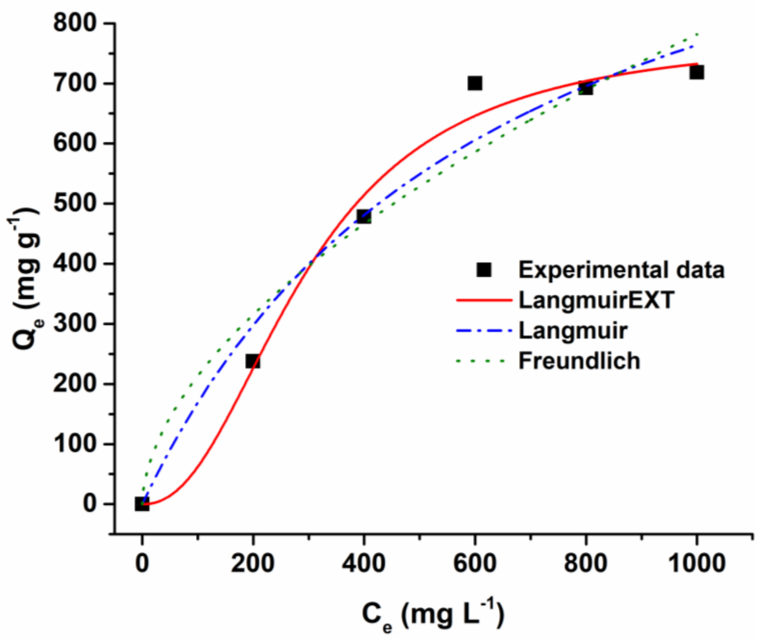

Fitting model	Parameter	correlation coefficient
LangmuirEXT	$Q_m = 781.4$ mg g^{-1} $K_S = 2.86 \times 10^{-6}$ $\gamma = 2.24$	$R^2 = 0.9730$
Langmuir	$Q_m = 1254.8$ mg g^{-1} $K_L = 1.56 \times 10^{-3}$	$R^2 = 0.9669$
Freundlich	$K_F = 15.90$ $n = 1.77$	$R^2 = 0.9474$

Figure S13. The adsorption isotherm of OG fitted with different models. As listed above, the correlation coefficient obtained from LangmuirEXT model is higher than other two models, suggesting LangmuirEXT model can well describe the adsorption process.

K. $Cr_2O_7^{2-}$ Adsorption Experiments

General procedure for $Cr_2O_7^{2-}$ adsorption experiments

Generally, **CON-1** (2 mg) was immersed into 6 mL $K_2Cr_2O_7$ aqueous solution (100 ppm), and the suspension was separated by centrifugation at different time points, then the upper clear solution was pipetted and measured by UV-Vis spectrophotometer. After each measurement, the solution was poured back to the initial vial to keep the total amount of sample constant. The $Cr_2O_7^{2-}$ content in the solution was calculated by comparing the maximum absorbance with the original $K_2Cr_2O_7$ solution. The kinetics data was fitted with pseudo-first order and pseudo-second order models respectively.

Pseudo-first order equation:

$$Q_t = Q_e - Q_e e^{-k_1 t}$$

Pseudo-second order equation:

$$Q_t = \frac{k_2 Q_e^2 t}{1 + k_2 Q_e t}$$

The adsorption capacity for $Cr_2O_7^{2-}$ was performed by immersing **CON-1** (5 mg) in 6 mL $K_2Cr_2O_7$ aqueous with different concentration (100 ppm, 200 ppm, 500 ppm, 800 ppm, and 1000ppm). After 4 hours, the adsorption reached equilibrium. By comparing the absorbance of $K_2Cr_2O_7$ solution before and after adsorption, the equilibrium adsorption capacity can be calculated. The adsorption isotherm of $Cr_2O_7^{2-}$ was fitted with LangmuirEXT, Langmuir, and Freundlich models respectively.

LangmuirEXT equation:

$$Q_e = \frac{Q_m K_S C_e^{\gamma}}{1 + K_S C_e^{\gamma}}$$

Langmuir equation:

$$Q_e = \frac{Q_m K_L C_e}{1 + K_L C_e}$$

Freundlich equation:

$$Q_e = K_F C_e^{1/n}$$

The recycle experiment was conducted by immersing **CON-1** (20 mg) in 60 mL $K_2Cr_2O_7$ aqueous solution (100 ppm). After the adsorption of $Cr_2O_7^{2-}$ is completed, the solution was analyzed by UV-Vis absorbance. The recycled material was obtained via filter and regenerated by soaking in same volume NaBr aqueous solution (33 g L^{-1}) for 5 hours. The regenerated **CON-1** was filtered and washed with water and ethanol. The regenerated **CON-1** was reused in next cycle, and the volume of $K_2Cr_2O_7$ aqueous solution was added according to the weight of collected material.

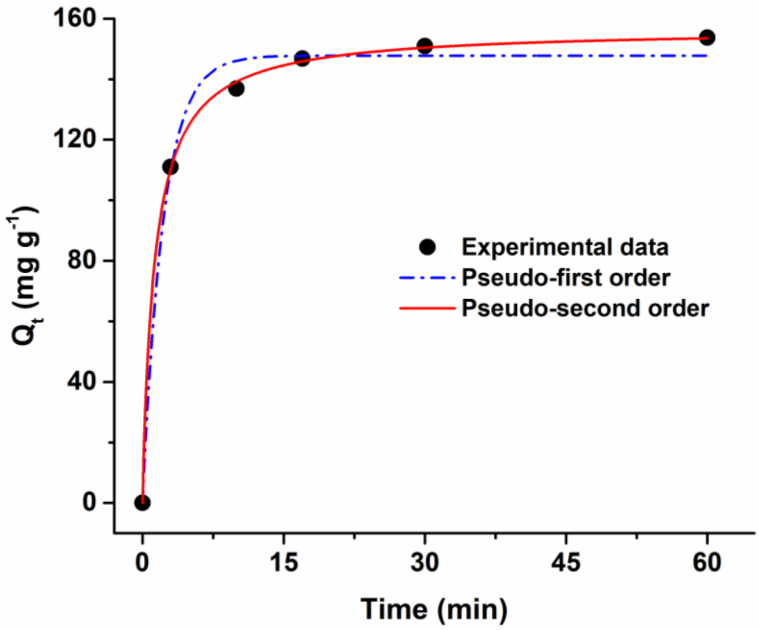

Fitting model	Parameter	correlation coefficient
Pseudo-first order	$Q_e = 147.8$ mg g^{-1} $k_1 = 0.452$ min^{-1}	$R^2 = 0.9924$
Pseudo-second order	$Q_e = 156.7$ mg g^{-1} $k_2 = 5.06 \times 10^{-3}$ g mg^{-1} min^{-1}	$R^2 = 0.9996$

Figure S14. The kinetics for adsorption of $Cr_2O_7^{2-}$. The data was fitted with pseudo-first order equation and pseudo-second order models respectively. As listed above, pseudo-second order fitting gave a higher correlation coefficient, indicating the adsorption of $Cr_2O_7^{2-}$ followed the pseudo-second order model.

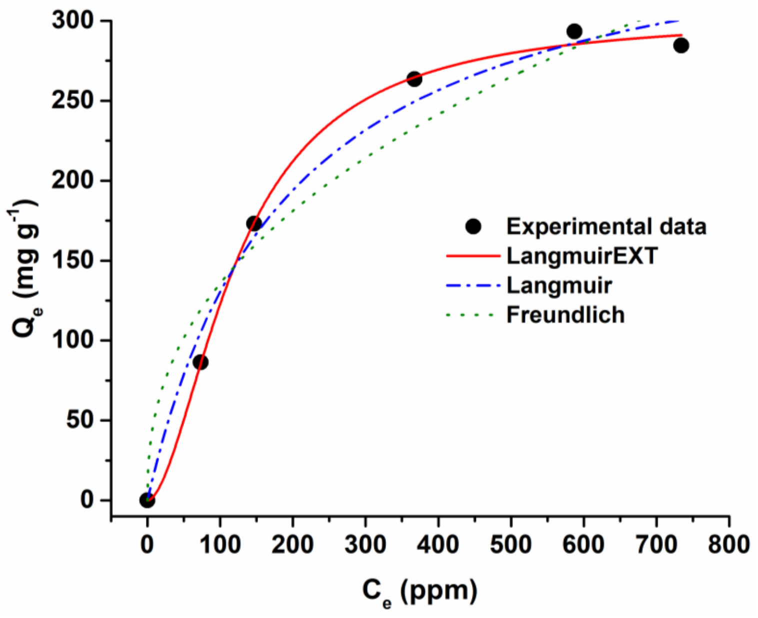

Fitting model	Parameter	correlation coefficient
LangmuirEXT	$Q_m = 303.6$ mg g^{-1} $K_S = 1.96 \times 10^{-4}$ $\gamma = 1.77$	$R^2 = 0.9966$
Langmuir	$Q_m = 378.8$ mg g^{-1} $K_L = 5.25 \times 10^{-3}$	$R^2 = 0.9869$
Freundlich	$K_F = 20.01$ $n = 2.41$	$R^2 = 0.9583$

Figure S15. The adsorption isotherm of $Cr_2O_7^{2-}$ fitted with different models. As listed above, the correlation coefficient obtained from LangmuirEXT model is higher than other two models, suggesting LangmuirEXT model can well describe the adsorption process.

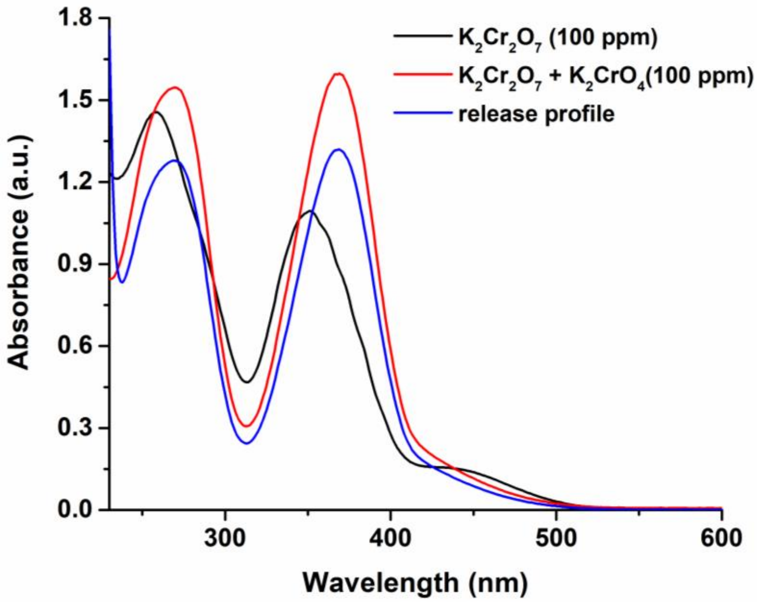

Figure S16. The release profile of $Cr_2O_7^{2-}$. In contrast to the profile of initial $K_2Cr_2O_7$ aqueous solution, the absorbance of the release profile exhibited some shift, which was attributed to partial conversion of $Cr_2O_7^{2-}$ to CrO_4.

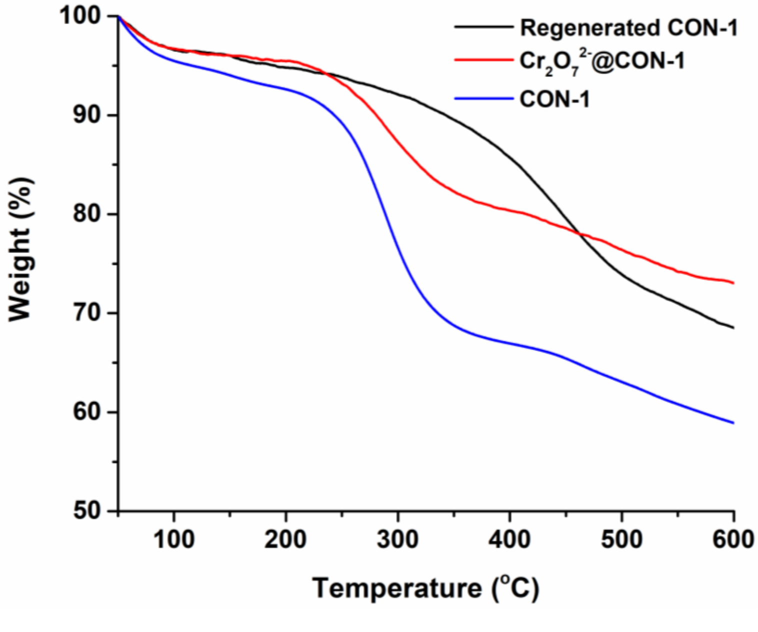

Figure S17. TGA curves of **CON-1**, **$Cr_2O_7^{2-}$@CON-1** and **Regenerated CON-1**.

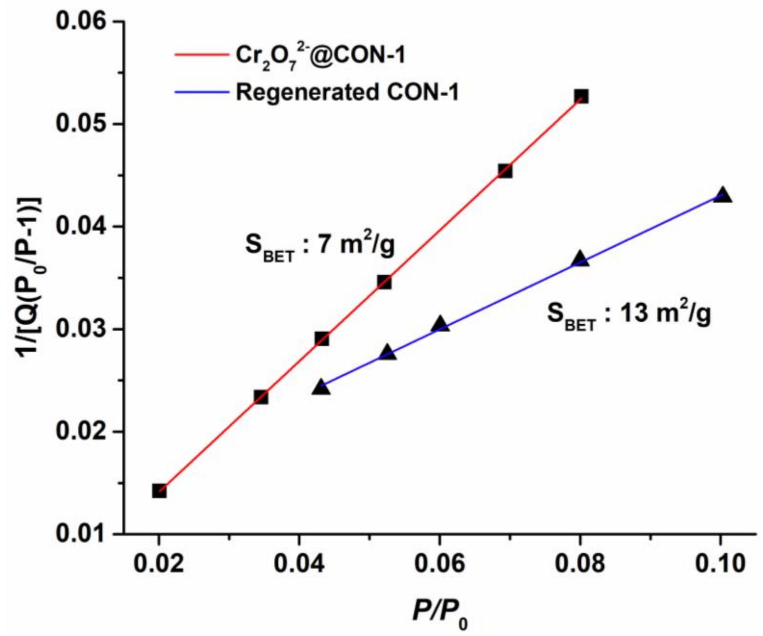

Figure S18. BET surface area plots for **$Cr_2O_7^{2-}$@CON-1** and **Regenerated CON-1** calculated from the adsorption isotherms.

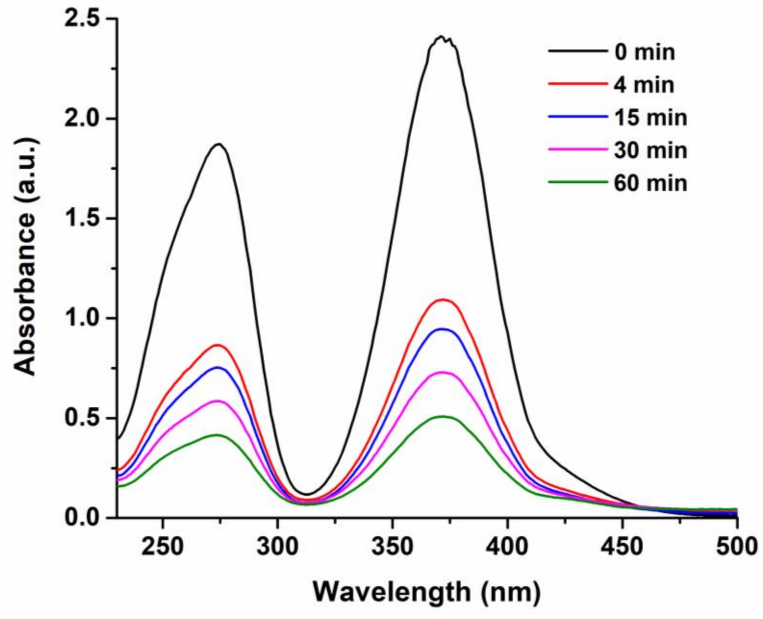

Figure S19. UV-Vis absorbance of K_2CrO_4 aqueous solution in the presence of **CON-1** in different intervals.

Table S2. Comparison of $Cr_2O_7{}^{2-}$ adsorption capacity of **CON-1** with other adsorbents.

Adsorbents	**Adsorption capacity (mg/g)**	**Ref.**
IMIP-Br	318	*J. Mater. Chem. A*, 2016, **4**, 12554.
ZJU-101	245	*Chem. Commun.*, 2015, **51**, 14732.
ABT·$2ClO_4$	214	*Angew. Chem., Int. Ed.*, 2013, **52**, 13769.
3	207	*Chem. Commun.* 2017,**53**, 9206.
L-SO_4	166	*Angew. Chem. Int. Ed.*, 2016, **55**, 7811.
1-Br	128	*Chem. Commun.* 2017*,* **53***,* 1860.
FIR-54	103.1	*Chem. Mater.*, 2015, **27**, 205.
2D-CP(1)	81.9	*Cryst. Growth. Des.* 2017*,* **17***,* 4437.
FIR-53	74.2	*ACS Nano*, 2014, **8**, 7451.
3D Dy-MOFs	62.9	*Chem. Commun.*, 2012, **48**, 8231.
PCN-134	57	*J. Am. Chem. Soc.*, 2016, **138**, 6636.
MOF-867	53.4	*Chem. Commun.*, 2015, **51**, 14732.
Porous organic polymers	172	*ACS Appl. Mater. Interfaces*, 2016, **8**, 18904.
NH_2-TNTs	154	*Chem. Eng. J.*, 2013, **225**, 153.
β-CD and quaternary ammonium groups modified cellulose	61	*J. Hazard. Mater.*, 2011, **187**, 303.
Modified magnetic chitosan chelating	58	*Int. J. Biol. Macromol.*, 2011, **49**, 513.
Calcined LDHs	17	*J. Am. Chem. Soc.*, 2011, **133**, 11110.
CON-1	**293**	***This work***